



DØnote 4855-CONF

Version:1.1
Author(s): Sinjini Sengupta

Send comments to d0-run2eb-021@fnal.gov
by March 12

**A Measurement of the $W \rightarrow \mu\nu$ Charge Asymmetry
with the DØ detector at $\sqrt{s} = 1.96$ TeV.**

The DØ Collaboration
(Dated: March 12, 2006)

A measurement of the muon charge asymmetry from W boson decays is presented. The asymmetry is measured using $\approx 230 \text{ pb}^{-1}$ of data collected between 2002 and 2004 with the DØ detector. The resultant distribution is compared with expectations from NLO calculations using the CTEQ6.1M and the MRST02 parton distribution functions and can be used as inputs to future PDF fits.

Preliminary Results for Winter 2006 Conferences

I. INTRODUCTION

A measurement of the W^\pm rapidity (y_W) distributions in $p\bar{p}$ collisions provides useful information about the parton distribution functions (PDF) of the u and d quarks in the proton. The PDFs are typically evaluated from Deep Inelastic Scattering experiments in the low x and high Q^2 region, where x is the momentum fraction carried by the partons in the hadron and Q^2 is the momentum transfer. In this measurement, the resonant production of the W boson constrains Q^2 to $\approx M_W^2$, where M_W is the mass of the W boson. Hence the region in phase space in x that this measurement can probe depends on the range of the rapidity of the W boson and is given by

$$x_{1(2)} = \frac{M_W}{\sqrt{s}} e^{(\pm)y_W}, \quad (1)$$

where $x_{1(2)}$ are the momentum fractions carried by the $u(d)$ quark, $(\pm)y_W$ are the positive and negative W boson rapidities that can be measured (for this analysis, $-2 < y_W < +2$) and \sqrt{s} is the center of mass energy. At $\sqrt{s} = 1.96$ TeV, this measurement probes the region in x between 0.005 and 0.3.

The W bosons at the Tevatron are primarily produced by quark-antiquark annihilation. Contributions from valence-valence and valence-sea annihilations amount to about 85% of the cross section [1] with the rest coming from sea-sea quark-antiquark annihilations. A W^+ is produced primarily by the interaction of a u quark from a proton and a \bar{d} quark from an antiproton and a W^- is produced primarily by the interaction of a d quark from a proton and a \bar{u} quark from an antiproton. Because u valence quarks carry on average more of the momentum of the proton than d valence quarks [2], the W^+ boson is boosted along the proton beam direction and the W^- boson along the antiproton beam direction, giving rise to the W production charge asymmetry.

It is difficult to measure the W^\pm rapidity due to the fact that the longitudinal momentum of the neutrino from the W decay cannot be measured directly. Instead, we access the same information by measuring the charge asymmetry of the W boson decay products [3]. In this analysis we use the muon decay channel. The muon asymmetry is a convolution of the W production charge asymmetry and the asymmetry from the $(V - A)$ decay. Since the $(V - A)$ asymmetry is well understood, the muon asymmetry is used to probe the parton distributions. The muon charge asymmetry is defined as

$$A(y_\mu) = \frac{\frac{d\sigma(\mu^+)}{dy} - \frac{d\sigma(\mu^-)}{dy}}{\frac{d\sigma(\mu^+)}{dy} + \frac{d\sigma(\mu^-)}{dy}}, \quad (2)$$

where $d\sigma(\mu^\pm)/dy$ is the cross section for the W^\pm decay muons as a function of muon rapidity. Taking the acceptance to be charge independent, and if the efficiencies, $\varepsilon_+(y)$ and $\varepsilon_-(y)$, for the positive and negative muons are different, the muon charge asymmetry can be written as:

$$A(y_\mu) = \frac{N_{\mu^+}(y) - kN_{\mu^-}(y)}{N_{\mu^+}(y) + kN_{\mu^-}(y)}, \quad (3)$$

where $k = \varepsilon_+(y)/\varepsilon_-(y)$ and $N_{\mu^\pm}(y)$ is the difference of the observed and estimated background muons for the rapidity bin y . In this analysis, the muon charge asymmetry is measured as a function of the pseudorapidity η , where η is defined as $-\ln[\tan(\theta/2)]$. In the relativistic limit, the rapidity y is the same as the pseudorapidity η .

The W charge asymmetry was measured by the CDF collaboration in both the electron and the muon channel in Run I [3 – 5] and in the electron channel only in Run II [6]. The addition of a central solenoid to the DØ detector in Run II enables the measurement of the charges of particles and allows a competitive measurement of the W charge asymmetry.

II. THE DØ DETECTOR

The Run II DØ detector is made up of a central tracker, a calorimeter and a muon detector [7]. The central tracker consists of a silicon microstrip tracker (SMT) and a central fiber tracker (CFT) which are both located within a 2T superconducting solenoid magnet. The SMT was designed to optimize tracking and vertexing within $|\eta| < 3$. The system has a six barrel longitudinal structure interspersed with 16 radial disks. The CFT has eight coaxial barrels, each supporting two doublets of overlapping scintillating fibers. One doublet serves as axial and the other, alternating by $\pm 3^\circ$, serves as stereo. Visible Light Photon Counters (VLPC) are used to convert the signal from optical to digital.

The sampling/constant calorimeter, made up of uranium and liquid argon, has a central section (CC) covering $|\eta| \approx 1$ and two end caps (EC) extending $|\eta| \approx 4$. The calorimeter is surrounded by the muon system consisting of

three layers of scintillators and drift tubes with one layer within the 1.8 T toroid and two layers without. Tracking at $|\eta| < 1$ relies on wide drift tubes while tracking at $1 < |\eta| < 2$ relies on mini drift tubes. Coverage for muons is partially compromised in the region $|\eta| < 1.25$ and $4.25 < \phi < 5.15$ rad by the calorimeter supports.

Luminosity is measured using plastic scintillator arrays located in front of the EC cryostats covering $2.7 < |\eta| < 4.4$. The trigger system at DØ is a three tier system which reduces the 1.7 MHz of data coming into the detector in three stages to 50 Hz that is written to tape.

DØ uses a right handed coordinate system with the proton beam defining the positive z direction. The origin of the coordinate system is at the center of the DØ system which roughly corresponds to the center of the interaction region. Physics η relates to the direction of travel and is measured with respect to the origin of the particle.

III. EVENT SELECTION: THE $W \rightarrow \mu\nu$ SIGNAL SAMPLE

Data recorded between August 2002 and March 2004, about 230 pb^{-1} , were used for this analysis. Events containing at least one muon were selected. All selected events were required to have fired one of the single muon triggers, either the “wide” trigger in the region $|\eta| < 1.4$ or the “all” trigger in the region $1.4 < |\eta| < 2.0$. Both triggers require hits in the muon detector at the first trigger level (L1), a local muon track with $p_T > 3$ GeV at the second trigger level (L2) and a track with $p_T > 10$ GeV at the third trigger level (L3). A ‘good’ muon was defined as

1. lying within the geometrical acceptance of the muon detector.
2. of at least ‘medium’ quality (where ‘medium’ is defined by the number of wire and scintillator hits in the muon system) and matched to a track in the central tracker and with track $p_T > 20$ GeV.
3. having a well reconstructed track with > 8 hits in the CFT, > 0 hits in the SMT and a track fit $\chi^2/\text{dof} < 3.3$ to ensure a low charge mis-identification rate.
4. not originating from cosmic rays, or within timing cuts of ± 10 ns in the scintillators of the innermost layer of the muon detector and with the distance of closest approach of the primary vertex from the beamspot $|\text{dca}| < 0.011$ cm.
5. not originating from a semi-leptonic decay, or isolated in both the calorimeter and the central tracker, where
 - (a) $\sum_{\text{etcone5}}(p_T) < 2.5$ GeV, where $\sum_{\text{etcone5}}(p_T)$ is the sum of the p_T of tracks within a cone around the muon with a radius $\Delta R = 0.5$, where $\Delta R = \sqrt{(\Delta\eta)^2 + (\Delta\phi)^2}$.
 - (b) $\sum_{\text{halo}}(E_T) = \sum_{\text{etcone4}}(E_T) - \sum_{\text{etcone1}}(E_T) < 2.5$ GeV, where $\sum_{\text{etcone4}}(E_T)$ and $\sum_{\text{etcone1}}(E_T)$ are the sum of calorimeter clusters around the muon in cones of radius $\Delta R = 0.4$ and $\Delta R = 0.1$ respectively. The coarse hadronic part of the calorimeter is not considered when calculating these sums.

In addition, the event was required to have $E_T > 20$ GeV and the W transverse mass $M_T > 40$ GeV (where $M_T = \sqrt{(\cancel{E}_T + p_T)^2 - (\cancel{E}_x + p_x)^2 - (\cancel{E}_y + p_y)^2}$ and p_T , p_x and p_y are the transverse, x and y components of the muon momentum). Further, to reduce the $Z \rightarrow \mu\mu$ background in the sample,

1. All events with a second medium muon, with or without a central track match, were rejected. To avoid vetoing on mis-reconstructed muons close to the original muon, the second muon was required to be at least $\Delta\phi > 0.1$ away from the original muon.
2. All events with a second good track, satisfying ‘good’ muon conditions 3 and 5 above, back to back with the muon track ($|\Delta\phi| > 2.1$) and with $p_T > 20$ GeV, were rejected.

There were 189697 W candidates selected after all the above selection cuts were applied to data.

IV. CHARGE MISIDENTIFICATION

The W charge asymmetry is sensitive to the misidentification of the charge of the muon. A positive muon misidentified as a negative muon would not only add to the number of negative muons but would also take away from the number of positive muons and vice versa. This dilutes the true asymmetry. The charge misidentification rate is estimated in data using a dimuon sample in which the events are required to fire one of the single muon triggers used for this analysis. Two medium, track-matched muons are selected and they are required to satisfy all of the muon

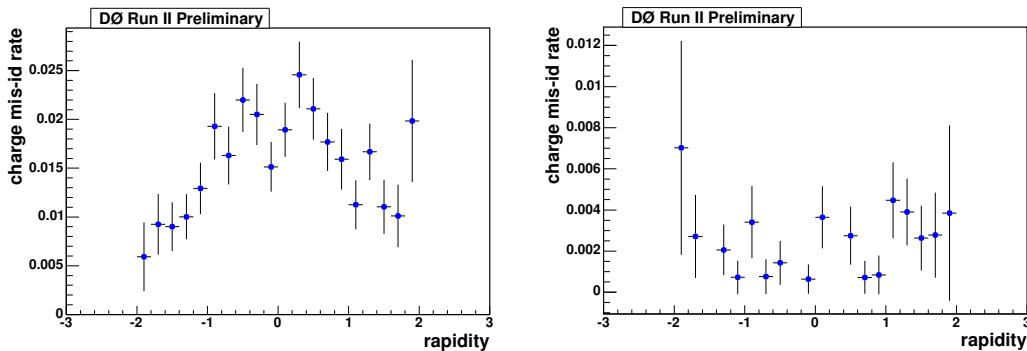


FIG. 1: The left plot shows the charge misidentification rate as a function of η when the events are selected without any track quality requirements whatsoever. The right plot shows the misidentification rate when the SMT and CFT hit requirements are applied.

and track selection cuts described above. Events with a dimuon invariant mass > 40 GeV are selected to form a Z sample. The charge misidentification rate is defined as

$$\text{charge misidentification rate} = \frac{N(\text{same sign})}{N(\text{same sign}) + N(\text{opposite sign})}. \quad (4)$$

The Z sample is found to contain 9958 events with only one event containing two same sign muons. Removing the dimuon invariant mass cut does not lead to an increase in the number of events with same sign muons. Neither does lowering the p_T cut on the muons from 20 to 15 GeV. In all cases, only the one event with two same sign muons is observed.

The charge misidentification rate is then verified using an independent dimuon sample where the events are required to fire one of a set of dimuon triggers. Out of 19284 Z events, there are 2 which are found to have same sign muons.

As a further test, all the track quality cuts were initially relaxed and the misidentification rate was checked by tightening the cuts one by one. Fig. 1 shows the misidentification rate decreasing as a function of η as the cuts are tightened.

The misidentification rate is also checked using a 594K GEANT Monte Carlo sample of $W \rightarrow \mu\nu$ events. The charge of the track at the generator level was compared to the charge of the reconstructed track. The charge misidentification rate in this sample is defined as

$$\text{charge misidentification rate} = \frac{N(q_{\text{gen}} \neq q_{\text{reco}})}{N(q_{\text{gen}} \neq q_{\text{reco}}) + N(q_{\text{gen}} = q_{\text{reco}})}. \quad (5)$$

Fig. 2 shows the charge misidentification rate as a function of η in the GEANT sample. The rate is found to be very low. Charge misidentification is therefore not expected to have any significant influence on the final charge asymmetry distribution. However, the charge misidentification rate of $(0.01 \pm 0.01)\%$ found in data is used to assign a systematic uncertainty to the muon charge asymmetry. Since the statistics are somewhat inconclusive at higher η , the systematic uncertainty for $|\eta| > 1.0$ is scaled by a factor of 5.0.

V. EFFICIENCIES

The W boson charge asymmetry can be measured as the difference divided by the sum of the number of positive and negative muons in each η bin (Eq. 4), corrected for the backgrounds, when the efficiencies for positively and negatively charged muons are the same. So it is important to check that there are no charge, p_T or η biases in the efficiencies. We look at the offline medium muon reconstruction efficiency, the L1-L2 muon trigger efficiency, the tracking efficiency, the L3 trigger efficiency and the isolation efficiency. The differences between the efficiencies of the positive and negative charges would contribute towards systematic uncertainties.

All the efficiencies are measured using the tag and probe method where a tag is chosen as a track matched isolated muon satisfying all the selection conditions. Then a probe is chosen as another track or another muon depending on

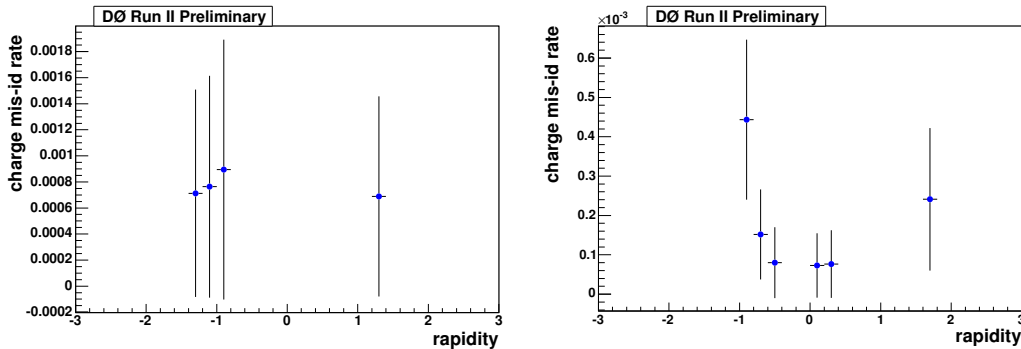


FIG. 2: The first plot shows the charge misidentification rate when the dca cut is applied in addition to the SMT and CFT hits requirement. The right plot shows the misidentification rate in Monte Carlo as a function of η .

the efficiency being measured. All the efficiencies were checked for biases as functions of p_T , charge and as functions of η with the charges separated out. The L1-L2 muon trigger efficiency was measured given the muon reconstruction efficiency while the L3 track trigger efficiency was measured given the tracking efficiency. No biases were observed due to charge or p_T .

The positive and negative efficiencies were then combined and studied in η in the following way.

$$\varepsilon_{\pm} = \varepsilon_{\pm}(\text{offline muon}) \times \varepsilon_{\pm}(\text{L2 muon}) \times \varepsilon_{\pm}(\text{offline track}) \times \varepsilon_{\pm}(\text{L3 track}) \quad (6)$$

Fig. 3 shows this combined efficiency distribution as a function of η with the efficiencies for the positive and negative charges separated out. The errors for each individual efficiency have been added in quadrature to give the errors for this distribution. Any correlations between muon identification and tracking that come into play while combining the efficiencies are second order effects and can be ignored.

The right plot in Fig. 3 shows the combined ratio between positive and negative efficiencies. This ratio is found to be constant as a function of η at the value of 0.99 ± 0.01 and with a $\chi^2/d.o.f.$ of 0.71. For the purpose of this analysis a value of $k = 1.0$ is used in Eq. 3 to calculate the W charge asymmetry, where $k = \varepsilon_+/\varepsilon_-$. The systematic uncertainties are evaluated by varying k by $\pm 1\sigma$ where $\sigma = 0.01$. The systematic uncertainties due to the variation of k are then propagated to the asymmetry.

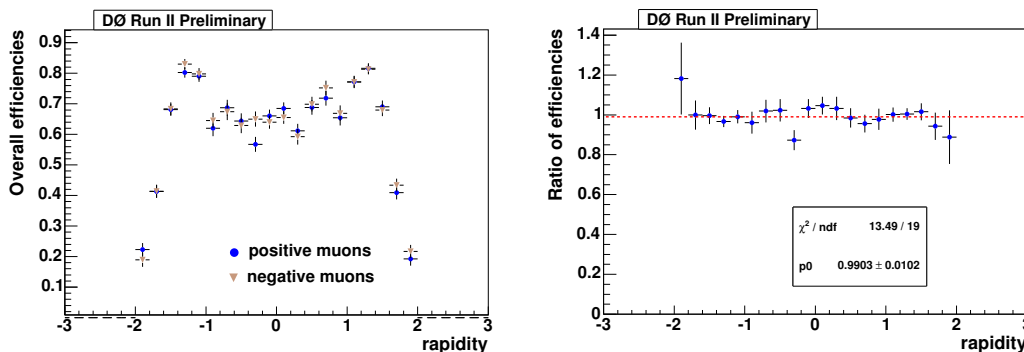


FIG. 3: Combined efficiency distributions by charge as a function of η on the left and the plot of the ratio of these efficiencies as a function of η fitted to a straight line on the right.

VI. OTHER BIASES

We also look for other possible sources of bias in the sample. We look at the raw asymmetry distribution for different solenoid and toroid polarities. The solenoid polarity influences the charge identification of tracks in the

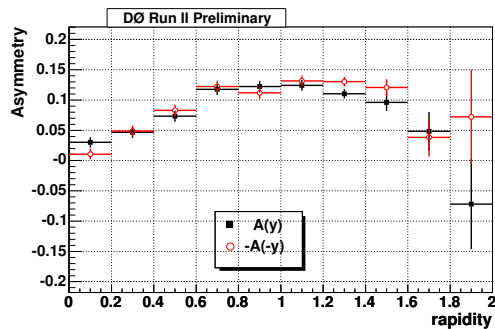


FIG. 4: The CP folded asymmetry. The points with the solid black squares represent the asymmetry for positive rapidity $A(y)$ while the points with the open red circles represent the asymmetry for the negative rapidity $-A(-y)$.

central tracker and can introduce a bias. The toroid polarity influences the muon trigger efficiencies and could be another source of bias. To increase statistics, the solenoid polarities have been studied independently from the toroid polarity and vice versa.

The asymmetries for the two solenoid polarities show good agreement between the forward and reversed solenoid field directions. The asymmetries for the two toroid polarities do not have as good an agreement but it was found that 50.7% of the selected W sample had forward toroid polarity while 49.3% had reverse toroid polarity. Any systematic uncertainties arising due to the difference in toroid polarities cancel. Moreover, since the differences between the positive and negative efficiencies due to the trigger and the tracking are used to estimate the systematic uncertainties, they include systematic effects due to the solenoid and toroid polarities.

We also check for possible detector effects by comparing the raw asymmetry distribution for positive and negative rapidities. Since the initial parton collisions are CP invariant, we expect to see agreement when folding over the asymmetry distribution such that $A(y) = -A(-y)$. No detector effects in rapidity were observed which needed correcting.

VII. MONTE CARLO SIMULATION USING PMCS

The Monte Carlo samples used to estimate the electroweak backgrounds in this analysis ($Z \rightarrow \mu\mu$, $Z \rightarrow \tau\tau$ and $W \rightarrow \tau\nu$ decays where $\tau \rightarrow \mu$) are first generated with the PYTHIA event generator [8] using the CTEQ6.1 PDF sets [9]. The detector resolution effects are then modeled using a Parameterized Monte Carlo Simulation (PMCS).

The energy deposited by the muon in the calorimeter is not modeled in PMCS. A simplified model of the calorimeter is externally used to simulate this effect. A systematic error is assigned to the asymmetry due to the uncertainties in the response of the calorimeter to minimum ionizing particles (MIP). Another source of systematic uncertainty comes from the error in the value of the hadronic energy scale that is used to smear the \cancel{E}_T in PMCS.

The isolation condition for muons is not modeled in PMCS. The isolation efficiency measured in data is therefore used to correct the Monte Carlo p_T distribution for isolation effects.

A. Isolation Efficiency

The isolation efficiency is measured in data using the tag and probe method in a sample of dimuon events where the tag is chosen as a track-matched isolated muon satisfying all track and muon selection requirements as described in Section 2.3 and the probe is chosen as a track-matched muon satisfying all of the same conditions except that it is not required to be isolated in either the tracker or the calorimeter. The fraction of isolated probe tracks with dimuon mass > 40 GeV give the efficiency.

The isolation efficiency is plotted as a function of p_T and η in Fig. 5. The efficiency appears to be constant for the charges in η . The efficiency in p_T is fitted to a constant value of 0.9209 ± 0.0018 with a $\chi^2/d.o.f. = 5.77$. An error, larger than the error in the fit, is assigned to the efficiency in order to make up for the bad χ^2 of the fit. This error was calculated by projecting the isolation efficiency distribution onto the y axis with weights assigned for the number of events in each bin of p_T . The mean of this distribution is the average isolation efficiency and it has an rms = 0.022. This value of the rms is assigned as the error in the isolation efficiency so that,

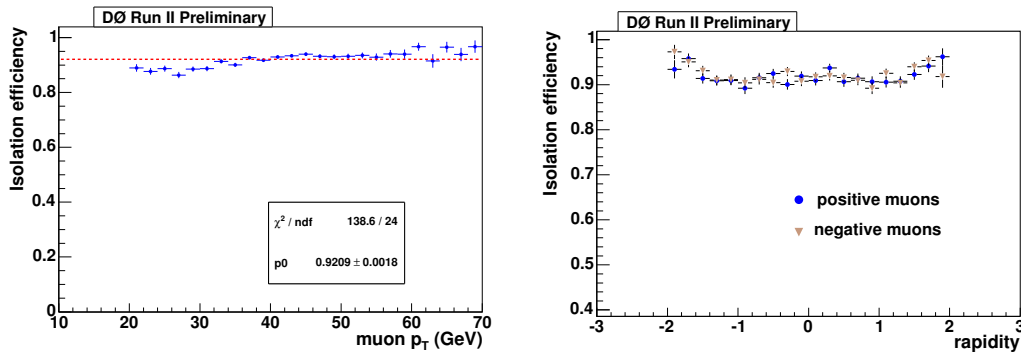


FIG. 5: The isolation efficiency plotted as a function of p_T on the left and as a function of η with the positive and negative charges separated out on the right.

$$\text{Isolation efficiency}(\varepsilon) = 0.92 \pm 0.02 . \quad (7)$$

The QCD background contamination in the data sample is evaluated from data using the Matrix method (see Section VIIB). One of the input parameters for the Matrix method is the signal isolation efficiency. The isolation efficiency measured in data is therefore also used as an input to the Matrix method.

VIII. BACKGROUND ESTIMATION

The largest source of contamination in the sample comes from electroweak backgrounds, $Z \rightarrow \mu\mu$, $W \rightarrow \tau\nu$ and $Z \rightarrow \tau\tau$ events. These backgrounds are estimated using Monte Carlo samples. The other major source of contamination in the sample is from quarks that decay semi-leptonically. This is the multijet background (referred to as the ‘QCD’ background) and is estimated from data. In order to extract the amount of electroweak background contamination in the data sample using Monte Carlo, it is necessary to normalize the signal + background Monte Carlo to data from which the QCD background has been subtracted. 500K $W \rightarrow \mu\nu$ signal Monte Carlo events were generated for each of the two triggers and smeared for detector effects as described earlier. 102384 events from the “wide” MC sample and 117717 events from the “all” MC sample passed the selection cuts.

A. Electroweak Backgrounds

1. The largest source of background in the W sample comes from $Z \rightarrow \mu\mu$ events in which one of the muons has not been reconstructed or lies outside the detector acceptance. The muon from a Z decay does not have a preferred direction as in the case of a muon from a W decay which dilutes the asymmetry. This background is estimated using 200K $Z/\gamma \rightarrow \mu^+\mu^-$ ($M_{Z/\gamma^*} > 30$ GeV) events simulated with PYTHIA and PMCS for each of the two triggers. The number of Z Monte Carlo events was scaled to the W signal Monte Carlo events using the SM ratio of the $Z \rightarrow \mu\mu$ to the $W \rightarrow \mu\nu$ cross section (0.092) and from the ratio of $Z/\gamma \rightarrow \mu^+\mu^-$ ($M_{Z/\gamma^*} > 30$ GeV) to $Z \rightarrow \mu^+\mu^-$ cross sections (1.30) [10]. 16239 events from the “wide” MC sample and 19057 events from the “all” MC sample passed the selection cuts.
2. $W \rightarrow \tau\nu$ events contribute to the contamination of the W sample when the tau decays to a muon and a neutrino. The muons from $W \rightarrow \tau\nu$ decays have an inherent asymmetry of their own which dilutes the true asymmetry. Correcting for the backgrounds bin by bin in η takes care of the inherent τ asymmetry. This background is estimated using 200K $W \rightarrow \tau\nu$ Monte Carlo events generated separately for the two triggers. 1071 events from the “wide” MC sample and 1256 events from the “all” MC sample passed the selection cuts.
3. There is also a contribution from $Z \rightarrow \tau\tau$ events in which one of the taus decays to a muon. This background is similarly estimated from 200K $Z \rightarrow \tau\tau$ Monte Carlo events (generated separately for the “wide” and the “all” triggers) which are normalized to the W sample just like the $Z \rightarrow \mu\mu$ sample. 742 events from the “wide” MC sample and 877 events from the “all” MC sample passed the selection cuts.

B. QCD Background

The QCD or multijet background, arising from quarks that decay semi-leptonically into muons, is estimated from data using the Matrix Method. The Matrix Method is simply two simultaneous equations which are used to extract the number of signal and background events in the sample.

A sample of events N_1 is selected, using all the selection cuts described in Section 2.3, except the isolation cut. The isolation criteria efficiently reject QCD background events and are used as the discriminator. The selected N_1 events contain B number of background events and S number of signal events. The isolation cut is then applied, resulting in the selection of N_2 events which is a subset of N_1 . The selected N_2 events is a combination of the number of signal and QCD background events which have passed the isolation cut.

$$N_1 = B + S, \quad (8)$$

$$N_2 = fB + \epsilon S, \quad (9)$$

where f is the efficiency for the background events to pass the isolation cut (or the fake rate) and ϵ is the efficiency for the signal events to pass the isolation cut (isolation efficiency). Solving the two equations we get the number of background events as

$$B = \frac{\epsilon N_1 - N_2}{\epsilon - f} \quad (10)$$

The isolation efficiency for signal events is 0.91 ± 0.01 as measured from data. The fake rate, or the isolation efficiency for background events, is obtained using low p_T data.

1. Fake Rate and QCD background estimation

The fake rate, or the efficiency of the background to pass the isolation cut, is estimated using a sample with all the selection cuts applied, except for the cuts on p_T and M_T and with $\cancel{E}_T < 10$ GeV. This sample is well separated from the signal sample. The fake rate for the sample is estimated to be

$$f = 0.11 \pm 0.02. \quad (11)$$

The amount of QCD background in the $W \rightarrow \mu\nu$ sample is then evaluated using the number of W events N_1 and N_2 , with and without the isolation requirement and Eq. 10, for each bin in η . The error in the fake rate contributes to the systematic uncertainty in the asymmetry.

C. Total Background

Table I shows the breakdown of all the backgrounds for the two single muon triggers, in the sample used for this analysis. To get the number of events for each type of background for the analysis, all the electroweak backgrounds (with proper scaling) were added to the number of events obtained from the $W \rightarrow \mu\nu$ signal Monte Carlo sample and this sum was normalized to the total number of W events obtained from data minus the calculated QCD background for the sample. This normalization is done over the range $|\eta| < 1.6$ for events which fire the “wide” trigger and $|\eta| < 2.0$ for events which fire the “all” trigger. The errors in each background are also similarly scaled for each bin in η . The scaled background errors are quadratically added to the error in data to get the total statistical error for each bin in η .

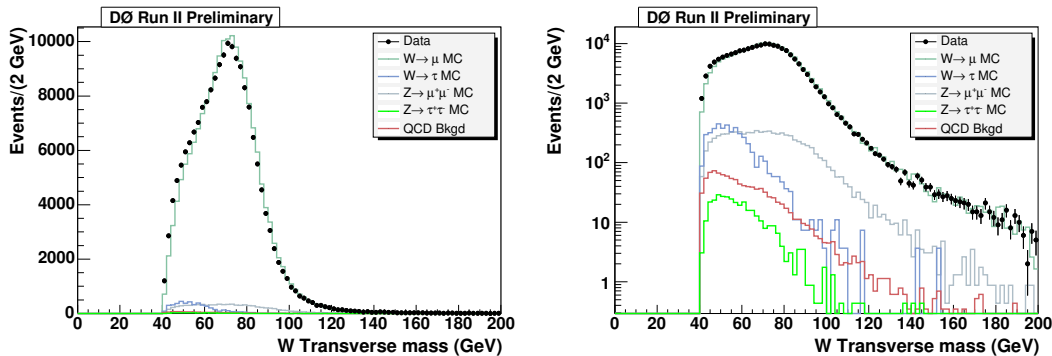
Fig. 6 shows the W transverse mass distribution with and without the log scale. This distribution shows the comparison between data and the total expected sum of (signal + background) Monte Carlo + QCD background for the “wide” and “all” triggers.

IX. COMBINING THE TRIGGERS

There were two single muon triggers used in this analysis, the “wide” ($|\eta| < 1.5$) and the “all” ($|\eta| < 2$) triggers. Monte Carlo samples modeling signal and background have been separately generated for each trigger and smeared

TABLE I: Summary of the estimated backgrounds in the W sample by trigger.

Background	“wide” trigger	“all” trigger
$Z \rightarrow \mu\mu$	$4.31 \pm 0.05\%$	$4.39 \pm 0.11\%$
$Z \rightarrow \tau\tau$	$0.19 \pm 0.01\%$	$0.20 \pm 0.02\%$
$W \rightarrow \tau\nu$	$2.32 \pm 0.02\%$	$2.43 \pm 0.08\%$
QCD	$2.77 \pm 0.04\%$	$2.76 \pm 0.09\%$

FIG. 6: The W transverse mass (data and Monte Carlo) in linear scale (left plot) and in log scale (right plot). The $W \rightarrow \mu\nu$ MC line is the sum of $W \rightarrow \mu\nu$ signal and $W \rightarrow \tau\nu$, $Z \rightarrow \mu\mu$, $Z \rightarrow \tau\tau$ and QCD.

for detector effects using PMCS. Using the “all” trigger for $|\eta| < 1.4$ or the “wide” trigger for $|\eta| > 1.6$ provides no significant gain in statistics and was not considered worthwhile. Since the “wide” trigger only goes out to $|\eta| < 1.5$, events which fire the “all” trigger in the η bin $1.4 - 1.6$ were used instead. This loss of statistics due to this was considered acceptable over the errors arising due to the systematic uncertainties and the scale factor from using both triggers in this bin.

X. RESULTS AND CONCLUSIONS

The muon charge asymmetry from the W decay is evaluated as a function of η using Equation 3. The asymmetry has been corrected for background effects on a bin-by-bin basis. Table III gives a breakdown of the asymmetry in bins of rapidity with the statistical and systematic uncertainties. Table IV gives a breakdown of the different systematic uncertainties in bins of rapidity. Table II gives the final values for the asymmetry and the total uncertainties on these values.

The final results are shown in Fig. 7. The plot on the left shows the asymmetry distribution which has been corrected for background effects. The yellow band shows the theoretical prediction for the W charge asymmetry at the parton level. This band was made using the NLO generator RESBOS-A and the CTEQ6.1M PDFs, with the 40 PDF error sets combined according to the recipe provided by the CTEQ collaboration [9]. The curve in red is the central value.

The plot on the right shows the folded asymmetry distribution. The positive and the negative rapidities were added for increased statistics. The results are compared to the theoretical predictions from the CTEQ6.1M PDFs (yellow band) and the MRST02 PDFs in blue. The statistical and systematic errors were combined. These are the first results for the W charge asymmetry from DØ and the first for the muon channel at the Tevatron in Run II.

The charge asymmetry is sensitive to the d/u ratio of the quark momentum distribution in the proton over the range $0.005 < x < 0.3$. In addition to the previous measurements made at hadron colliders, this muon charge asymmetry measurement can help further constrain the PDFs, especially where the value of the calculated asymmetry deviates from the predicted asymmetry and has errors smaller than the PDF errors. More specifically, this measurement can help reduce the errors on some of the parameters that go into the PDFs and that are the most sensitive to this measurement.

This measurement is complimentary to the CDF electron asymmetry analysis [6] due to the different systematic uncertainties. As this measurement was made with a p_T cut for the muon lower than the p_T cut used in the electron analysis and because the amplitude of the asymmetry depends on the lepton p_T , this measurement can provide

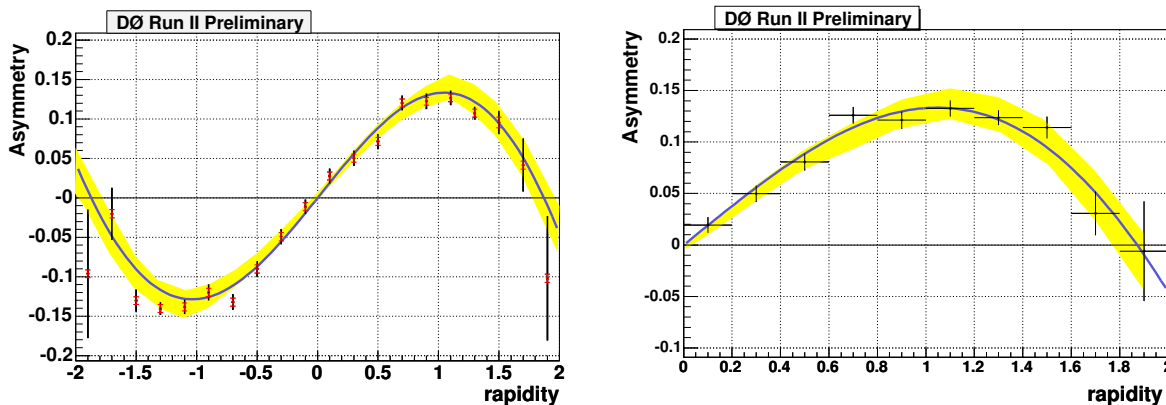


FIG. 7: The left plot shows the corrected muon charge asymmetry distribution with the statistical errors in black and the systematic errors in red. The yellow band is the envelope determined using the 40 CTEQ6.1 PDF error sets. The blue line is the asymmetry using the MRST02 PDF. The right plot shows the corrected and CP folded muon charge asymmetry with combined statistical and systematic uncertainties.

TABLE II: Total uncertainties on the folded asymmetry in bins of rapidity.

Rapidity(l)	Rapidity(u)	asymmetry	total error
0.0	0.2	0.019	0.0076
0.2	0.4	0.049	0.0079
0.4	0.6	0.081	0.0080
0.6	0.8	0.126	0.0081
0.8	1.0	0.121	0.0083
1.0	1.2	0.133	0.0078
1.2	1.4	0.124	0.0072
1.4	1.6	0.114	0.0106
1.6	1.8	0.031	0.0213
1.8	2.0	-0.006	0.0484

additional useful information about the PDFs.

This measurement is not yet systematics limited because the statistical uncertainties are greater than the systematic uncertainties in every bin. This bodes well for the future of this analysis as more data collected by the DØ detector is analyzed.

-
- [1] R. Hamberg *et al.*, Nucl. Phys. B **359**, 343 (1991).
 - [2] E. L. Berger, F. Halzen, C. S. Kim and S. Willenbrock, Phys. Rev. D **40**, 83 (1989); A. D. Martin, R. G. Roberts and W. J. Stirling, Mod. Phys. Lett. A **4**, 1135 (1989).
 - [3] F. Abe *et al.*, Phys. Rev. Lett. **68**, 10 (1992).
 - [4] F. Abe *et al.*, Phys. Rev. Lett. **74**, 850 (1995).
 - [5] F. Abe *et al.*, Phys. Rev. Lett. **81**, 5754 (1998).
 - [6] D. Acosta *et al.*, Phys. Rev. D **71**, 051104 (2005).
 - [7] “The Upgraded DØ Detector”, V.M. Abazov *et al.* (DØ Collaboration), submitted to Nucl. Instr. and Methods, hep-physics/0507191.
 - [8] T. Sjöstrand *et al.*, Comp. Phys. Commun. 135, p238(2001), “PYTHIA v6.2 Physics Manual.”
 - [9] J. Pumplin, D. R. Stump, J. Huston, H. L. Lai, P. Nadolsky and W. K. Tung, JHEP **0207**, 012 (2002).
 - [10] S. Frixione and B. R. Webber, JHEP **0206**, 029 (2002); JHEP **0308**, 007 (2003).

TABLE III: Statistical and systematic uncertainties on the asymmetry in bins of rapidity.

Rapidity(l)	Rapidity(u)	asymmetry	statistical uncertainty	systematic uncertainty
-2.0	-1.8	-0.096	0.0816	0.0050
-1.8	-1.6	-0.020	0.0332	0.0052
-1.6	-1.4	-0.130	0.0139	0.0050
-1.4	-1.2	-0.140	0.0081	0.0049
-1.2	-1.0	-0.138	0.0092	0.0052
-1.0	-0.8	-0.120	0.0103	0.0053
-0.8	-0.6	-0.132	0.0099	0.0051
-0.6	-0.4	-0.090	0.0098	0.0053
-0.4	-0.2	-0.049	0.0096	0.0053
-0.2	0.0	-0.011	0.0092	0.0050
0.0	0.2	0.028	0.0093	0.0050
0.2	0.4	0.050	0.0097	0.0050
0.4	0.6	0.071	0.0096	0.0051
0.6	0.8	0.120	0.0095	0.0050
0.8	1.0	0.122	0.0100	0.0050
1.0	1.2	0.127	0.0094	0.0050
1.2	1.4	0.107	0.0080	0.0051
1.4	1.6	0.095	0.0149	0.0067
1.6	1.8	0.041	0.0336	0.0051
1.8	2.0	-0.102	0.0789	0.0053

TABLE IV: Breakdown of the systematic uncertainties by bins of rapidity.

Rap(l)	Rap(u)	Eff ratio k	Isolation eff	'MIP' val p	fake rate	H.E.S.	charge misid
-2.0	-1.8	0.0050	0.0002	0.0006	0.0001	0.0003	0.0005
-1.8	-1.6	0.0049	0.0003	0.0003	0.0011	0.0011	0.0005
-1.6	-1.4	0.0047	0.0006	0.0006	0.0004	0.0003	0.0005
-1.4	-1.2	0.0048	0.0002	0.0004	0.0002	0.0007	0.0005
-1.2	-1.0	0.0048	0.0016	0.0003	0.0001	0.0001	0.0005
-1.0	-0.8	0.0049	0.0003	0.0002	0.0001	0.0010	0.0001
-0.8	-0.6	0.0049	0.0008	0.0007	0.0008	0.0002	0.0001
-0.6	-0.4	0.0049	0.0005	0.0003	0.0004	0.0012	0.0001
-0.4	-0.2	0.0050	0.0003	0.0001	0.0005	0.0011	0.0001
-0.2	0.0	0.0051	0.0002	0.0004	0.0001	0.0003	0.0001
0.0	0.2	0.0051	0.0007	0.0003	0.0001	0.0005	0.0001
0.2	0.4	0.0050	0.0001	0.0003	0.0001	0.0003	0.0001
0.4	0.6	0.0049	0.0004	0.0002	0.0001	0.0004	0.0001
0.6	0.8	0.0047	0.0006	0.0005	0.0001	0.0015	0.0001
0.8	1.0	0.0049	0.0005	0.0002	0.0007	0.0012	0.0001
1.0	1.2	0.0048	0.0002	0.0002	0.0002	0.0001	0.0005
1.2	1.4	0.0051	0.0005	0.0002	0.0004	0.0005	0.0005
1.4	1.6	0.0050	0.0010	0.0005	0.0005	0.0045	0.0005
1.6	1.8	0.0050	0.0002	0.0001	0.0008	0.0002	0.0005
1.8	2.0	0.0051	0.0011	0.0006	0.0013	0.0003	0.0005